UDC 628.4 https://doi.org/10.20998/2074-272X.2026.1.03

Z. Ayache, O. Dahou

Development of a NARX neural network for a tribo-aero-electrostatic separator with rotating disk electrodes

Introduction. *The exponential growth of waste electrical and electronic equipment (WEEE) requires efficient strategies for plastic waste management. Plastics, a major fraction of WEEE, represent both an environmental challenge due to low biodegradability and a valuable source of secondary raw materials.* ***Problem.*** *Tribo-aero-electrostatic separators with rotating disk electrodes offer a promising solution for fine plastic separation. However, their performance depends on multiple, nonlinear, and time-varying factors such as disk speed, voltage, and particle properties. These complex interactions make analytical modeling and stable process control difficult, limiting industrial implementation. The* ***goal*** *of this work is to develop a reliable dynamic model based on NARX neural networks capable of predicting the real-time evolution of key process variables such as recovered mass and particle charge.* ***Methodology.*** *The proposed NARX neural network learns temporal nonlinear relationships directly from experimental data, avoiding the need for explicit physical equations. Experiments were conducted on a synthetic 50:50 mixture of Acrylonitrile Butadiene Styrene (ABS) and Polystyrene (PS) particles (500-1000 μm) to assess model performance under varying disk speeds, voltages, and air flow rates.* ***Results.*** *The developed model accurately predicts the recovered mass and acquired charge of both ABS and PS over a wide range of operating conditions. The predictions show strong agreement with experimental measurements, maintaining low error levels even at parameter extremes.* ***Scientific novelty.*** *This work represents the first application of NARX neural networks to model the dynamic behavior of a two-rotating-disk tribo-aero-electrostatic separator. The approach captures essential time-dependent interactions that conventional static or analytical models fail to describe.* ***Practical value.*** *The NARX model exhibits high predictive accuracy and robustness across an extended operating domain (4–20 kV, 15–60 rpm, 7–9 m^3/h), with errors limited to the 10^{-3} g and 10^{-3} μC ranges. These characteristics demonstrate its potential for real-time intelligent control and adaptive optimization of electrostatic separation processes in plastic waste recycling.* References 39, tables 3, figures 9.
Key words: **electrostatic separation, high voltage, dynamic modeling, NARX neural network, recycling.**

Вступ. *Експоненціальне зростання кількості відходів електричного та електронного обладнання (WEEE) вимагає ефективних стратегій управління пластиковими відходами. Пластики, основна частина WEEE, становлять як екологічну проблему через низьку біорозкладність, так і цінне джерело вторинної сировини.* ***Проблема***. *Трибоаероелектростатичні сепаратори з обертовими дисковими електродами пропонують перспективне рішення для тонкого розділення пластику. Однак їхня продуктивність залежить від численних, нелінійних та змінних у часі факторів, таких як швидкість диска, напруга та властивості частинок. Ці складні взаємодії ускладнюють аналітичне моделювання та стабільне керування процесом, обмежуючи промислове впровадження.* ***Метою*** *роботи є розробка надійної динамічної моделі на основі нейронних мереж NARX, здатних прогнозувати еволюцію ключових змінних процесу, таких як відновлена маса та заряд частинок, у реальному часі.* ***Методологія***. *Запропонована нейронна мережа NARX вивчає часові нелінійні залежності безпосередньо з експериментальних даних, уникаючи необхідності явних фізичних рівнянь. Експерименти проводилися на синтетичній суміші частинок акрилонітрилбутадієнстиролу (ABS) та полістиролу (PS) у співвідношенні 50:50 для оцінки продуктивності моделі за різних швидкостей дисків, напруг та швидкостей потоку повітря.* ***Результати***. *Розроблена модель точно прогнозує відновлену масу та набутий заряд як ABS, так і PS у широкому діапазоні робочих умов. Прогнози демонструють високу відповідність з експериментальними вимірюваннями, підтримуючи низький рівень похибки навіть при екстремальних значеннях параметрів.* ***Наукова новизна***. *Ця робота являє собою перше застосування нейронних мереж NARX для моделювання динамічної поведінки трибоаероелектростатичного сепаратора з двома обертовими дисками. Цей підхід враховує важливі залежні від часу взаємодії, які звичайні статичні або аналітичні моделі не можуть описати.* ***Практична значимість***. *Модель NARX демонструє високу прогностичну точність та стійкість у розширеній робочій області (4–20 кВ, 15–60 об/хв, 7–9 $м^3$/год), з похибками, обмеженими діапазонами 10^{-3} г та 10^{-3} мкКл. Ці характеристики демонструють його потенціал для інтелектуального керування в режимі реального часу та адаптивної оптимізації процесів електростатичного розділення при переробці пластикових відходів.* Бібл. 39, табл. 3, рис. 9.
Ключові слова: **електростатична сепарація, висока напруга, динамічне моделювання, нейронна мережа NARX, переробка.**

Introduction. The management of plastic waste from electrical and electronic equipment (WEEE) has become a global priority in the face of the exponential growth of such waste and the environmental challenges they pose. Plastics, which account for a significant portion of WEEE streams, represent a major problem due to their low biodegradability and their impact on ecosystems when not properly recycled [1, 2]. The recycling of these plastics offers both economic and environmental opportunities, allowing for a reduction in their impact while meeting the growing demand for secondary raw materials [3].

In this context, several electrostatic separation devices have been developed in research laboratories [4–6]. The tribo-electrostatic separator with two rotating disks, in particular, has shown high efficiency in sorting submillimetric granular mixtures, where charging occurs in a fluidized bed containing the material mix to be separated. In this system, a pair of electrodes in the form of two rotating stainless steel disks, driven by a variable-speed motor and connected to high-voltage power supplies with opposite polarities, is immersed to generate an intense electric field [7, 8].

However, the performance of this process is strongly influenced by a combination of nonlinear, interacting, and time-varying factors, including disk rotational speed, applied voltage, particle charge, and air flow rate [9]. Moreover, environmental factors (such as relative humidity and temperature of ambient air) influence the separation process [10–12]. These dependencies make process behavior highly dynamic and sensitive to perturbations, resulting in difficulties in maintaining stable and optimal separation conditions. This complexity limits the industrial application of separators due to the difficulty in maintaining optimal performance in a stable manner [13].

Consequently, it becomes essential to develop dynamic models capable of accurately describing the transient behavior of tribo-aero-electrostatic separators

and predicting their performance under varying operational conditions. The design of advanced control systems for such devices relies on the availability of internal models able to capture their nonlinear and time-dependent dynamics. Traditional analytical and phenomenological modeling approaches, while useful for simplified cases, fail to adequately describe these complex dynamics, particularly when multiple coupled parameters evolve simultaneously in time [14].

In this context, artificial intelligence (AI) offers a powerful and innovative alternative. Artificial neural networks (ANNs), in particular, have emerged as tools of choice for modeling and identifying complex processes [15–19]. Unlike traditional approaches, neural networks do not require explicit knowledge of the underlying physical relationships. They are capable of learning directly from experimental data by identifying complex nonlinear relationships between input and output variables. This learning ability makes them particularly well-suited for multifactorial processes where interactions are difficult to model analytically.

ANNs have been effectively used to model and optimize electrostatic separation processes. For instance, in roll-type electrostatic separation, ANNs combined with genetic algorithms have been employed to maximize insulation product yield by optimizing control variables such as high voltage and roll electrode speed [20]. In the context of industrial electrostatic separators with rotating electrodes, ANNs facilitate multicriterion optimization, addressing the complexity of adjusting control variables in dynamic industrial environments [21, 22]. ANNs also play a crucial role in predicting the performance of electrostatic separation in food waste recovery, demonstrating high accuracy in aligning experimental and predicted results [23].

Nevertheless, most ANN-based models reported in the literature remain static or empirical, which limits their ability to represent the temporal evolution and dynamic interactions inherent to electrostatic separation systems. This limitation is particularly critical for tribo-aero-electrostatic separators with rotating electrodes, where the charging, transport, and separation of particles evolve over short and long time scales [24]. To overcome these limitations, this study focuses on the development and validation of a Nonlinear Autoregressive with Exogenous Inputs (NARX) neural network model designed to capture the dynamic behavior of a tribo-aero-electrostatic separator equipped with two rotating disk electrodes operating under high-voltage conditions**.** The NARX structure, known for its ability to represent systems with memory and feedback, has demonstrated strong performance in modeling nonlinear time-series processes [25–28], making it particularly suitable for this application.

The **goal** of this work is to develop a reliable dynamic model based on NARX neural networks capable of predicting the real-time evolution of key process variables such as recovered mass and particle charge. Experiments are carried out on a synthetic 50:50 mixture of acrylonitrile butadiene styrene (ABS) and polystyrene (PS), two representative thermoplastic polymers of WEEE streams, with particle sizes ranging from 500 to 1000 μm. The dataset is acquired through a LabVIEW based data acquisition system, allowing accurate and real-time monitoring of operational parameters such as disk rotational speed, applied voltage, and air flow rate.

Materials and methods. A tribo-aero-electrostatic separator equipped with two rotating disk electrodes (Fig. 1) was used for this study. In this device, the separation of fine granular materials is achieved under the combined influence of electrostatic and aerodynamic forces. Granular materials are first introduced into a fluidized bed inside the separation chamber, where repeated particle–particle and particle–wall collisions induce tribo-electric charging**.** Simultaneously, a controlled air flow maintains the particles in suspension, ensuring homogeneous mixing and frequent collisions. Inside the chamber, two stainless-steel disk electrodes rotate at adjustable seeds and are polarized by high-voltage supplies of opposite polarity.

Fig. 1. Tribo-aero-electrostatic separator with two rotating disks: 1 – control panel; 2 – variable speed DC motors; 3 –vibrating feeder; 4 – cylindrical feeder; 5 – separation chamber with two rotating disk electrodes; 6 – Faraday cages; 7 – balances; 8 – blower; 9 – electrometers (Keithley 6514); 10 – portable colorimeter NH310; 11 – computer [7]

The charged particles are driven toward the electrode of opposite sign and adhere to its surface under the combined effect of electrostatic and aerodynamic forces (Fig. 2). Brushes or scrapers then detach the particles from the disks and direct them to separate collectors. Less-charged or neutral particles remain suspended until they acquire sufficient charge to be collected [29].

Fig. 2. Collection of insulating particles in the two-rotating-disk tribo-aero-electrostatic separator

Previous investigations on this separator configuration have demonstrated its capability to selectively sort fine polymer mixtures and confirmed the strong influence of parameters such as electrode voltage, disk speed, and air flow rate on separation efficiency [24,

30–33]. Building upon these findings, the present work extends the analysis toward continuous operation and dynamic modeling to support the development of a data-driven predictive model based on NARX neural networks. The material mixture used consists of two polymer types: brown ABS and white PS (∅0.5–1 mm), supplied by APR2 (France), a company specializing in WEEE recycling (Fig. 3). The studied mixture is balanced (50 % ABS / 50% PS) and continuously fed by a vibratory mechanism. According to their positions in the tribo-electric series, ABS becomes positively charged while PS becomes negatively charged, and they are collected respectively by the negative and positive electrodes [30].

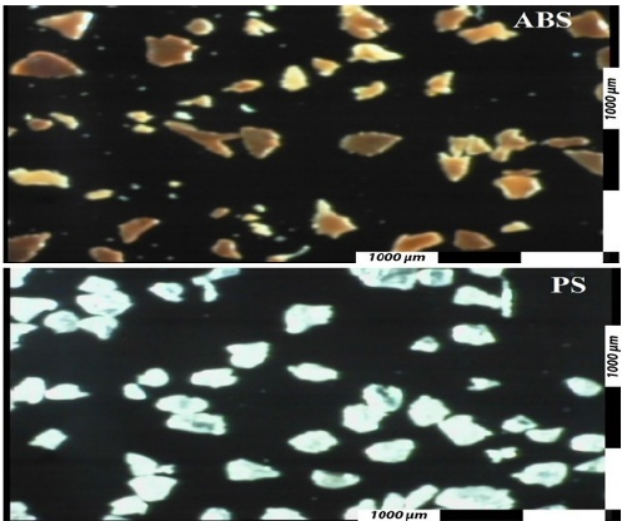

Fig. 3. Micrographs of ABS and PS particles composing the studied materials

The separator is equipped with a monitoring and control panel that enables real-time acquisition of key operating data: high-voltage levels, disk rotation speed, fan speed, and air flow rate. Separated materials are gathered in Faraday-type tanks connected to Keithley 6514 electrometers and placed on electronic balances (0.1 g resolution, 2 kg capacity). Measurements of electric charge and mass are recorded through a LabVIEW based data acquisition system. All experiments are conducted under controlled ambient conditions (relative humidity 40–50 %, temperature 17–21 °C).

The data collected in this study come from multiple experimental series as described in [31]. The effect of high voltage was evaluated in experiments conducted at a fixed disk rotational speed of 30 rpm and a constant air flow rate of 8 m^3/h, for voltages of ±4 kV, ±8 kV, ±12 kV, ±16 kV, and ±20 kV. In the second series of experiments, the disk rotational speed was successively adjusted to 15 rpm, 30 rpm, 40 rpm, 50 rpm, and 60 rpm, while maintaining a constant voltage of ±12 kV and an air flow rate of 8 m^3/h. Finally, a separation experiment was carried out with the fluidization air flow rate varied by adjusting the blower speed to 7 m^3/h, 7.5 m^3/h, 8 m^3/h, 8.5 m^3/h, and 9 m^3/h, at a constant rotational speed of 30 rpm and voltage of ± 12 kV.

The resulting dataset, composed of synchronized time-series measurements of mass and charge, served as the basis for training and validating the proposed NARX neural network model.

Architecture and implementation of the NARX neural network. There are currently several types of ANNs used in various applications [32]. In this work, we focus specifically on the NARX neural network model, which is a type of recurrent neural network well suited for modeling nonlinear systems, particularly time series [33]. Figure 4 illustrates the topology of the NARX network defined in study. The equation defining the NARX model is as follows:

$$y(t+1)=f[y(t),\dots y(t-d_y+1);u(t),\dots,u(t-d_u+1)], \quad (1)$$

where $u(t)$, $y(t)$ are the input and output of the network at time t; d_u, d_y are the input and output orders; f is the nonlinear function.

Equation (1) can be expressed in vector form as:

$$\boldsymbol{y}(t+1)=f[\boldsymbol{y}(t);\boldsymbol{u}(t)]. \quad (2)$$

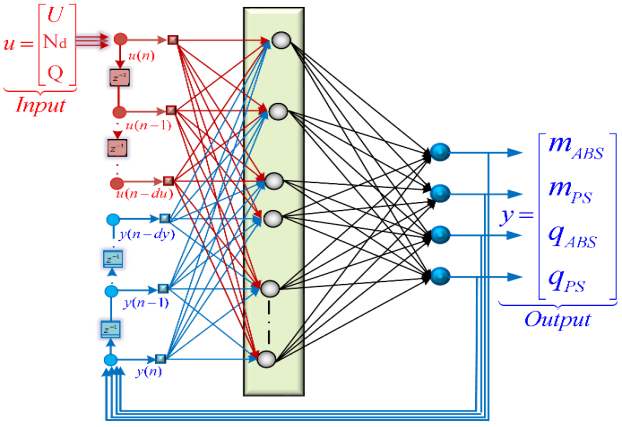

Fig. 4. NARX neural network with delayed input

The input vector $\boldsymbol{u}=[U,\ N_d,\ Q]^T$ consists of 3 elements: the high voltage applied to the electrodes (U), the rotational speed of the electrodes (N_d) and the air flow rate of the blower (Q); T is the transpose of the vector. In contrast, the output vector $\boldsymbol{y}$ = $[m_{ABS},\ m_{PS},\ q_{ABS},\ q_{PS}]^T$ consists of 4 elements: the collected mass of ABS and BS (m_{ABS}, m_{PS}) and the electrical charge of the collected mass of ABS and PS (q_{ABS}, q_{PS}). This network also employs tapped delay lines to store previous values of the input sequence $\boldsymbol{u}(t)$ and output sequence $\boldsymbol{y}(t)$. Moreover, the NARX network output, $\boldsymbol{y}(t)$, is fed back to the network input (through delays), since $\boldsymbol{u}(t)$ depends on $y(t–1)$, $y(t–2),\dots,y(t–d_y)$. However, for efficient training, this feedback loop can be opened.

To optimize the training conditions of the network, data preprocessing is highly recommended. Therefore, all data used for training and testing are normalized within the range [–1, +1]. This normalization helps reduce training time while improving the network's performance [34]. The dataset is typically divided into training, validation, and, if available, test sets, with common splits of 70/30 or 70/15/15 [35]. For temporally correlated data, block-wise segmentation is required to preserve the dynamics, with each subset including at least one complete cycle.

In this study, the entire dataset of mass and mass charge measurements collected in the previous section was used to train the NARX network in order to determine the optimal number of neurons in the hidden layer. These dynamic data consist of a total of 6950 measurement points, of which 70 % (4864 points) were

used for training and 30 % (2086 points) for testing, to validate the performance of the NARX neural network. The model characteristics are summarized in Table 1, and the implementation was carried out in MATLAB using the Neural Network Toolbox.

Table 1

Structure of the studied neural network

Neural network type	NARX
Training algorithm	Levenberg-Marquardt
Initialization algorithm	Nguyen-Widrow
Hidden neurons activation function	Hyperbolic tangent
Output neurons activation function	Identity

There is no universal rule to determine the optimal neural network structure (number of layers, number of neurons, types of connections) or its parameters (activation functions, input delays, feedback delays). An iterative process, inspired by previous work [36–39], was implemented to optimize the NARX network structure. This process determines the number of neurons in the hidden layer as well as the delays on the inputs and feedback outputs by testing various configurations and selecting the best one based on a performance criterion.

Based on the above, the search for the optimal structure was conducted using the parameters listed in Table 2.

Table 2

NARX network parameters

Search range of number of neurons (NN) in the hidden layer	[5, 30]
Search range for the number of input delays	[1, 3]
Search range for the number of output delays	[1, 6]
Number of reinitializations per configuration	10
Total number of final reinitializations	50

The selection of the optimal model is based on the mean squared error (MSE) given by (3) and the maximum coefficient of determination (R-squared), which defines the goodness of fit of the experimental data (4), mean error (ME) (5) and mean absolute error (MAE) (6):

$$MSE = \sum_{i}^{N} (\boldsymbol{M}_i - \boldsymbol{Y}_i)^2 \Big/ N ; \quad (3)$$

$$R^2 = 1 - \sum_{i}^{N} (\boldsymbol{M}_i - \boldsymbol{Y}_i)^2 \Big/ \sum_{i}^{N} (\boldsymbol{M}_i - \overline{\boldsymbol{Y}}_i)^2 ; \quad (4)$$

$$ME = \sum_{i}^{N} (\boldsymbol{M}_i - \boldsymbol{Y}_i) \Big/ N_e ; \quad (5)$$

$$MAE = \sum_{i}^{N} |\boldsymbol{M}_i - \boldsymbol{Y}_i| \Big/ N , \quad (6)$$

where N is the number of samples used for training; N_e is the number of experiments performed for each variation parameter; $\boldsymbol{M_i}$ is the measured value; $\bar{\boldsymbol{Y}}_i$ is the average output; $\boldsymbol{Y_i}$ is the output provided by the network.

The total number of configurations tested is 540 (30×3×6). Each configuration is tested 10 times, and the best one is tested again 50 times, resulting in a total of 5,450 training runs (540×10+50) (Fig. 5). The search for the optimal structure was performed on a machine equipped with an Intel® Core™ i7-11800X 2.3 GHz processor. The optimization results are shown in Table 3. Using 24 hidden neurons, an input delay of 1 step, and an output delay of 2 steps achieves the best performance.

Table 3

Results of the optimal structure search

Number of neurons (NN) in the hidden neurons	24
Input delays	1
Output delays	3
Number of elements	169
MSE	$21.2 \cdot 10^{-6}$
R^2	>0.9999

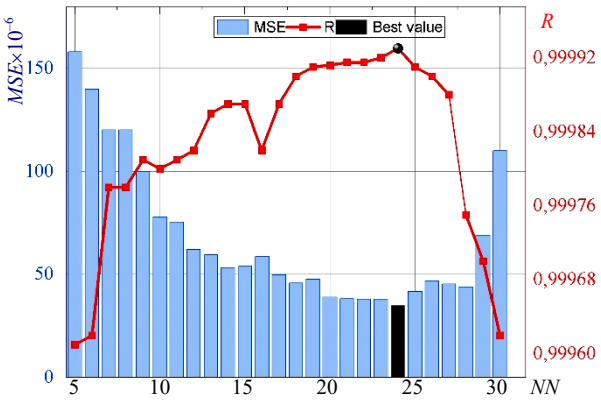

Fig. 5. Performance of the NARX network as a function of the number of neurons in the hidden layer

In Fig. 6 the graphs *a*, *b*, *e* and *f* show the model prediction results at different voltages (4–20 kV). The train and test training data, represented by a circle symbol and blue and black discontinuous line, are compared to the data predicted by the NARX network, represented by a cross symbol and red and orange solid line.

Visual inspection reveals exceptional agreement between experimental measurements and model predictions across all voltage levels. Both recovered mass (Fig. 6,*a*,*b*) and acquired charge (Fig. 6,*e*,*f*) show a strong positive correlation with applied voltage, following expected physical principles of electrostatic separation. The nearly perfect overlap between prediction curves and experimental data demonstrates the model's capability to capture the underlying system dynamics without explicit physical modeling.

Quantitative analysis confirms this observational assessment. The average prediction errors remain below 0,035 for mass recovery (Fig. 6,*c*,*d*) and 0,05 for charge acquisition (Fig. 6,*g*,*h*) across the entire voltage range. Notably, the model maintains its predictive accuracy for both training and testing data sets, indicating excellent generalization capabilities without over fitting. The slight error increase at voltage extremes (particularly at 4 kV) can be attributed to signal-to-noise ratio challenges in low-intensity separation conditions.

The investigation of disk rotational speed influence (Fig. 7) shows that, unlike the applied voltage, this parameter does not exert a significant effect on particle recovery. Across the full range of tested speeds (15–60 rpm), the collected masses remain nearly constant, with variations within ±2 g for ABS and ±3 g for PS, indicating that rotational speed is not a critical factor in the overall separation performance.

The NARX model accurately reproduces this insensitivity. In the test dataset, the mean error (ME) is around 5.5 mg for ABS and 7 mg for PS, while for the charges it remains limited to $\pm 9 \cdot 10^{-3}$ μC.

A temporal analysis, however, reveals transient fluctuations up to $8 \cdot 10^{-3}$ at the beginning of the sequences, reflecting the short-term instability induced by particle motion initiation and air flow turbulence in the fluidized bed. These fluctuations quickly decay, and the prediction errors converge back to zero in the steady-state regime.

The comparison between training and validation datasets highlights a remarkable consistency, as the errors remain of the same order of magnitude in both cases. This robustness confirms that the NARX model not only captures the overall stability of the process but also its transient regimes, while reinforcing the finding that disk rotational speed does not significantly influence the recovery outcome.

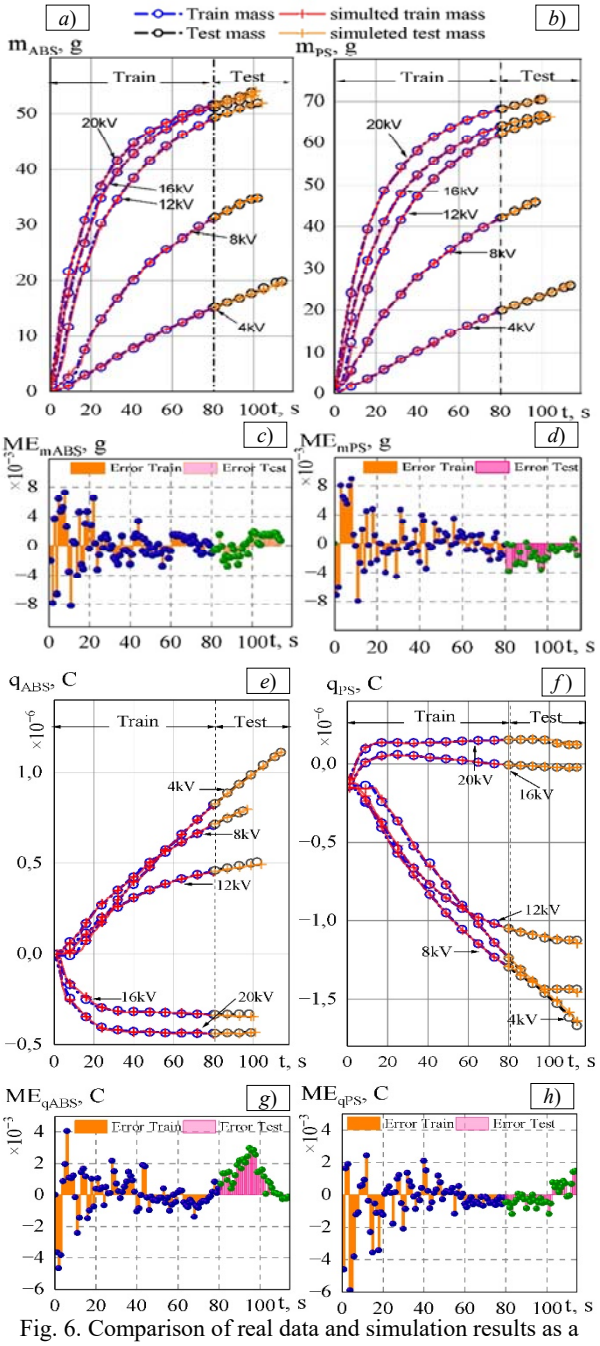

Fig. 6. Comparison of real data and simulation results as a function of high voltage variation: recovered ABS (*a*) and PS (*b*) mass; average error at each measured point for ABS (*c*) and PS (*d*) mass; recovered ABS (*e*) and PS (*f*) charge; average error at each measured point for ABS (*g*) and PS (*h*) charge

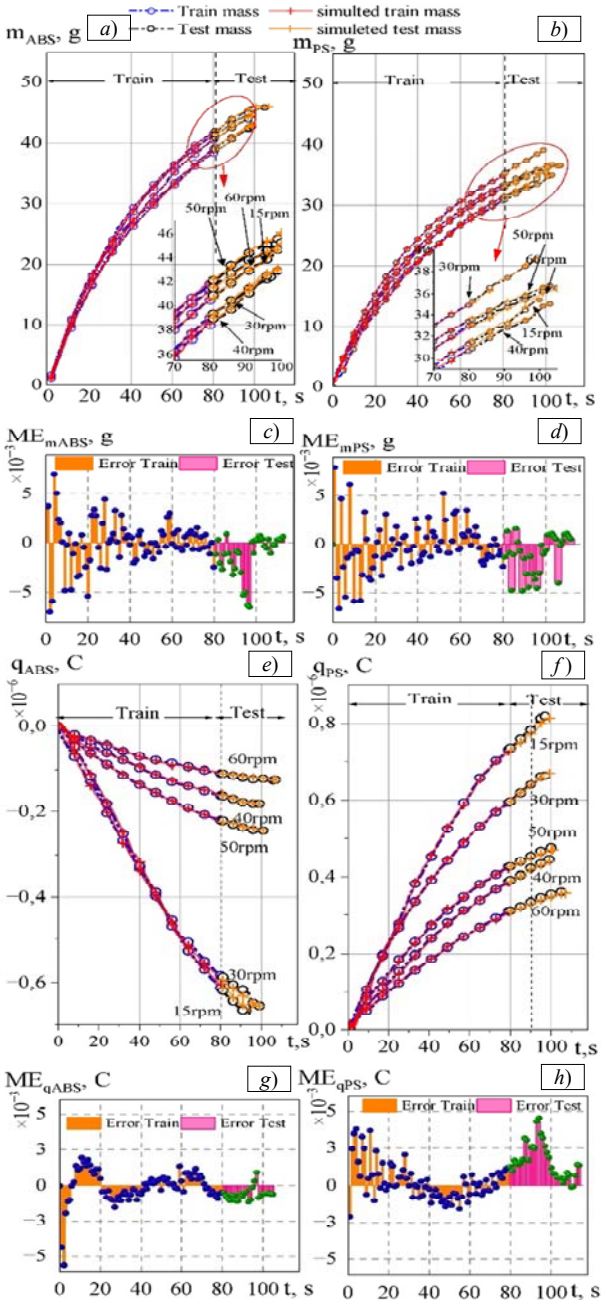

Fig. 7. Comparison of real data and simulation results as a function of variation of disk rotational speed: recovered ABS (*a*) and PS (*b*) mass; average error at each measured point for ABS (*c*) and PS (*d*) mass; recovered ABS (*e*) and PS (*f*) charge; average error at each measured point for ABS (*g*) and PS (*h*) charge

The investigation of air flow rate influence (Fig. 8) shows that this parameter has a noticeable effect on the recovery of both ABS and PS particles. As the air flow increases from 7 to 9 m^3/h, the collected masses exhibit measurable variations, reflecting the direct role of fluidization intensity on particle suspension and residence time. The NARX model accurately captures these dynamics. In the test dataset, ME remains within 4.2 mg for ABS and 6.8 mg for PS, while charge prediction errors are confined to $\pm 9 \cdot 10^{-3}$ μC. A temporal analysis highlights transient fluctuations of about $7.8 \cdot 10^{-3}$ at the beginning of the sequences, attributed to turbulence effects and rapid redistribution of particles when air flow is modified. These deviations quickly stabilize, and the

errors converge toward values close to zero once steady-state conditions are reached.

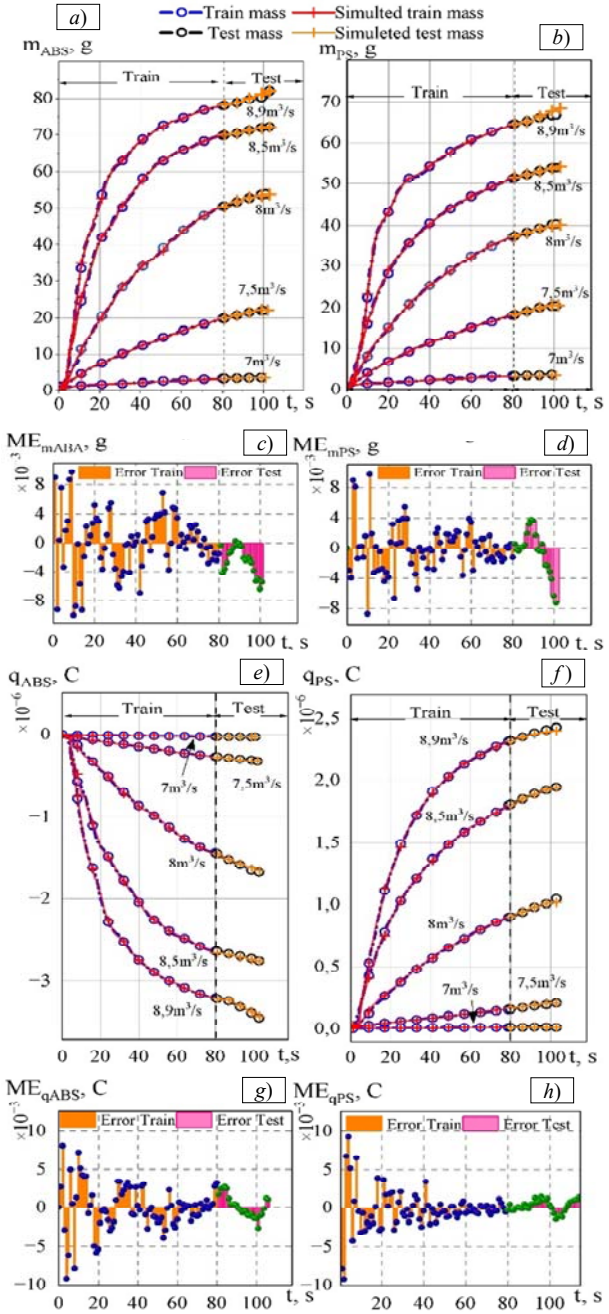

Fig. 8. Comparison of real data and simulation results as a function of air flow rate: recovered ABS (*a*) and PS (*b*) mass; average error at each measured point for ABS (*c*) and PS (*d*) mass; recovered ABS (*e*) and PS (*f*) charge; average error at each measured point for ABS (*g*) and PS (*h*) charge

Figure 9 shows MAE for the prediction of recovered mass and acquired charge of ABS and PS materials, as a function of voltage, disk rotational speed, and air flow rate, with a distinction between training and testing data.

The results show that the NARX model provides good accuracy during the training phase, with low MAE values for all variables. In the tests, slight increases in error appear at the extreme values of the parameters, reflecting sensitivity to extrapolation. For ABS, the errors are more pronounced for electrical charge prediction, especially at high air flow rates, where they reach values of 7.75 mC and 8.88 mC for air flow values of 8.5 m^3/h and 8.9 m^3/h, respectively. This is probably due to unmodeled complex electrostatic phenomena. PS shows better stability, especially for mass prediction (it does not exceed 9.6 mg, see Fig. 9,*b*), although errors also slightly increase under reaches 9.5 mg for test data (see Fig. 9,*c*).

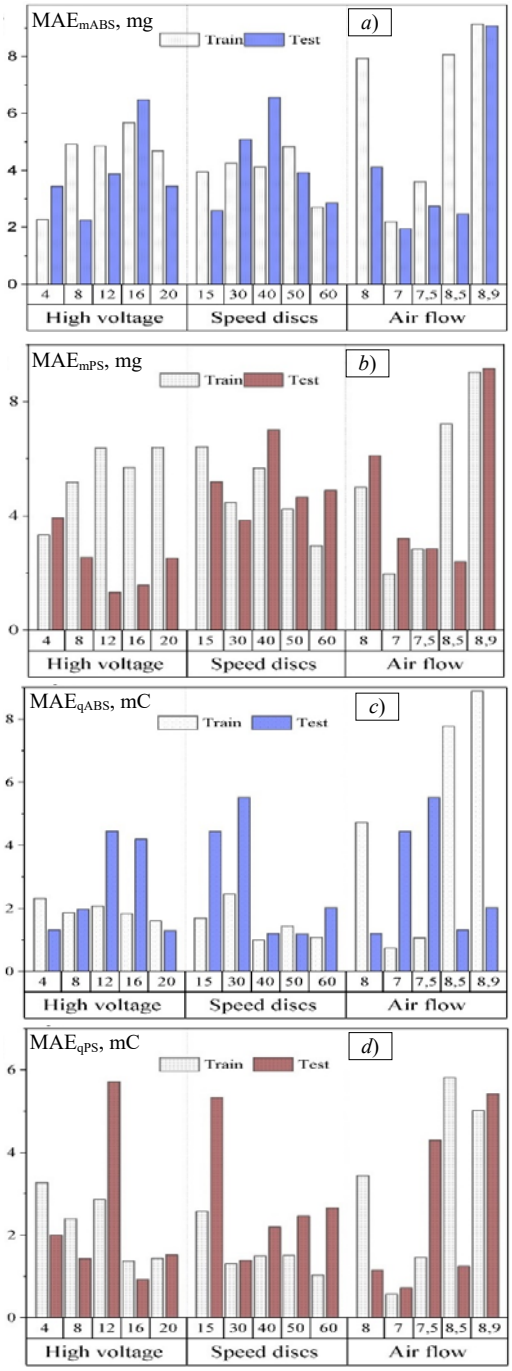

Fig. 9. MAE of predicted mass and charge for ABS and PS as functions of voltage, disk speed, and air flow rate (training vs. testing data): MAE of the predicted ABS (*a*) and PS (*b*) mass; MAE of the predicted ABS (*c*) and PS (*d*) charge

The main contribution of Fig. 9 lies in its ability to precisely identify the model's weak spots, without undermining its overall robustness. Indeed, MAE values remain largely within acceptable limits, even during testing, confirming that the NARX model provides a reliable approximation of the system's behavior over a wide range of operating conditions.

Conclusions. In this work, a NARX neural network has been developed and applied to model the dynamic behavior of a two-rotating-disk tribo-aero-electrostatic separator operating under high-voltage electric fields**.** The proposed model considers key process variables, including applied voltage, disk rotational speed, and air flow rate, as inputs, while the predicted outputs are the recovered mass and the acquired electrical charge of the separated particles.

The main objective of the study was to develop a dynamic model capable of accurately reproducing the nonlinear and time-dependent behavior of the separation process, thereby overcoming the limitations of traditional static or empirical approaches. The dynamic and recurrent structure of the NARX network enables it to capture complex temporal interactions between electrical, aerodynamic, and tribo-electric phenomena. The model was trained and tested using time-series data collected under multiple experimental conditions, allowing a thorough evaluation of its generalization capability.

Quantitative validation results confirm the high predictive accuracy and robustness of the proposed approach. Across the full operating range (4–20 kV, 15–60 rpm, 7–9 m^3/h), the ME for mass prediction remains below 5.5 mg for ABS and 7 mg for PS, while the MAE for charge prediction is limited to $\pm 9 \cdot 10^{-3}$ μC. Even at extreme conditions (e.g., ±4 kV or high air flow rates), the model maintains acceptable accuracy, with maximum deviations not exceeding 9.6 mg for mass and 8.9 μC for charge, confirming its robustness to parameter variations.

From a scientific standpoint, this work represents the first application of a NARX neural network to the dynamic modeling of a tribo-aero-electrostatic separator equipped with two rotating disk electrodes**.** The model successfully bridges the gap between analytical modeling and real-time predictive intelligence, providing a reliable foundation for further system optimization.

From a practical perspective, the robustness of the model across a wide range of operating conditions (4–20 kV, 15–60 rpm, 7–9 m^3/h) confirms its suitability for integration into intelligent control architectures for industrial electrostatic separation processes.

Future research will focus on developing a closed-loop control strategy that leverages the NARX model to optimize separation efficiency in real time**.** Such an intelligent control system will enable adaptive process regulation and enhanced operational stability in industrial plastic recycling applications.

Conflict of interest. The authors declare that they have no conflicts of interest.

REFERENCES

1. Geyer R., Jambeck J.R., Law K.L. Production, use, and fate of all plastics ever made. *Science Advances*, 2017, vol. 3, no. 7, art. no. e1700782. doi: https://doi.org/10.1126/sciadv.1700782.

2. Menad N., Guignot S., van Houwelingen J.A. New characterisation method of electrical and electronic equipment wastes (WEEE). *Waste Management*, 2013, vol. 33, no. 3, pp. 706-713. doi: https://doi.org/10.1016/j.wasman.2012.04.007.

3. Gundupalli S.P., Hait S., Thakur A. A review on automated sorting of source-separated municipal solid waste for recycling. *Waste Management*, 2017, vol. 60, pp. 56-74. doi: https://doi.org/10.1016/j.wasman.2016.09.015.

4. Daiku H., Inoue T., Tsukahara M., Maehata H., Kakeda K. Electrostatic separation technology for waste plastics-development of a high-purity type separator for plastics. *Proceedings Second International Symposium on Environmentally Conscious Design and Inverse Manufacturing*, 2001, pp. 562-565. doi: https://doi.org/10.1109/ECODIM.2001.992424.

5. Zenkiewicz M., Zuk T. Physical basis of tribocharging and electrostatic separation of plastics. *Polimery*, 2014, vol. 59, no. 04, pp. 314-323. doi: https://doi.org/10.14314/polimery.2014.314.

6. Mach F., Adam L., Kacerovský J., Karban P., Doležel I. Evolutionary algorithm-based multi-criteria optimization of triboelectrostatic separator. *Journal of Computational and Applied Mathematics*, 2014, vol. 270, pp. 134-142. doi: https://doi.org/10.1016/j.cam.2014.02.009.

7. Mekhalef Benhafssa A., Medles K., Boukhoulda M.F., Tilmatine A., Messal S., Dascalescu L. Study of a Tribo-Aero-Electrostatic Separator for Mixtures of Micronized Insulating Materials. *IEEE Transactions on Industry Applications*, 2015, vol. 51, no. 5, pp. 4166-4172. doi: https://doi.org/10.1109/TIA.2015.2434794.

8. Tilmatine A., Benabboun A., Brahmi Y., Bendaoud A., Miloudi M., Dascalescu L. Experimental Investigation of a New Triboelectrostatic Separation Process for Mixed Fine Granular Plastics. *IEEE Transactions on Industry Applications*, 2014, vol. 50, no. 6, pp. 4245-4250. doi: https://doi.org/10.1109/TIA.2014.2319584.

9. Achouri I.-E., Boukhoulda M.-F., Medles K., Richard G., Zeghloul T., Dascalescu L. Electrostatic Separation of Tribocharged Granular Mixtures of Two or More Plastics Originating From WEEE. *IEEE Transactions on Industry Applications*, 2022, vol. 58, no. 6, pp. 7701-7708. doi: https://doi.org/10.1109/TIA.2022.3197544.

10. Achouri I.-E., Dani C., Zeghloul T., Lungu M., Dascalescu L. Effect of ambient humidity on the tribo-electrostatic separation of granular plastic wastes. *Particulate Science and Technology*, 2024, vol. 42, no. 6, pp. 908-914. doi: https://doi.org/10.1080/02726351.2023.2295399.

11. Benabderrahmane A., Dani C., Medles K., Zeghloul T., Tomasella F., Lungu M., Dascalescu L., Parenty A. Effect of storage at different levels of relative humidity of ambient air on the tribo-electrostatic separation of granular plastics containing brominated flame retardants. *IEEE Transactions on Industry Applications*, 2023, pp. 1-6. doi: https://doi.org/10.1109/TIA.2023.3272872.

12. Dani C., Achouri I.-E., Zeghloul T., Aouimeur D., Lungu M., Dascalescu L. Triboelectric Charging and Electrostatic Separation of Granular Plastic Wastes Exposed to Long-Term Action of High Levels of Ambient Humidity. *IEEE Transactions on Industry Applications*, 2025, vol. 61, no. 1, pp. 1194-1201. doi: https://doi.org/10.1109/TIA.2024.3462902.

13. Achouri I.E., Zeghloul T., Richard G., Medles K., Nouri H., Dscalescu L. Premises for industrial application of a two-rotating-disks-type tribo-aero-electrostatic separator for micronized WEEE. *2017 IEEE Industry Applications Society Annual Meeting*, 2017, pp. 1-4. doi: https://doi.org/10.1109/IAS.2017.8101697.

14. Carlson R. Design of Experiments, Principles and Applications, L. Eriksson, E. Johansson, N. Kettaneh- Wold, C. Wikström and S. Wold, Umetrics AB, Umeå Learnways AB, Stockholm, 2000, ISBN 91-973730-0-1, xii + 329 pp. *Journal of Chemometrics*, 2001, vol. 15, no. 5, pp. 495-496. doi: https://doi.org/10.1002/cem.686.

15. Nelles O. *Nonlinear System Identification. From Classical Approaches to Neural Networks, Fuzzy Models, and Gaussian Processes*. Springer, 2020. 1225 p. doi: https://doi.org/10.1007/978-3-030-47439-3.

16. Haykin S. *Neural Networks and Learning Machines. 3rd Ed.* Pearson Publ., 2008. 936 p.

17. Bengharbi A.A., Laribi S., Allaoui T., Mimouni A. Photovoltaic system faults diagnosis using discrete wavelet transform based artificial neural networks. *Electrical Engineering & Electromechanics*, 2022, no. 6, pp. 42-47. doi: https://doi.org/10.20998/2074-272X.2022.6.07.
18. Vasilevskij V.V., Poliakov M.O. Reproducing of the humidity curve of power transformers oil using adaptive neuro-fuzzy systems. *Electrical Engineering & Electromechanics*, 2021, no. 1, pp. 10-14. doi: https://doi.org/10.20998/2074-272X.2021.1.02.
19. Rouaibia R., Djeghader Y., Moussaoui L. Artificial neural network and discrete wavelet transform for inter-turn short circuit and broken rotor bars faults diagnosis under various operating conditions. *Electrical Engineering & Electromechanics*, 2024, no. 3, pp. 31-37. doi: https://doi.org/10.20998/2074-272X.2024.3.04.
20. Touhami S., Medles K., Dahou O., Tilmatine A., Bendaoud A., Dascalescu L. Modeling and Optimization of a Roll-Type Electrostatic Separation Process Using Artificial Neural Networks. *IEEE Transactions on Industry Applications*, 2013, vol. 49, no. 4, pp. 1773-1780. doi: https://doi.org/10.1109/TIA.2013.2256451.
21. Dahou O., Medles K., Touhami S., Boukhoulda M.F., Tilmatine A., Dascalescu L. Application of Genetic Algorithms to the Optimization of a Roll-Type Electrostatic Separation Process. *IEEE Transactions on Industry Applications*, 2011, vol. 47, no. 5, pp. 2218-2223. doi: https://doi.org/10.1109/TIA.2011.2161851.
22. Dahou O., Touhami S., Ayache Z. Optimal control of an industrial electrostatic rotating electrode separator using artificial intelligence technics. *Przegląd Elektrotechniczny*, 2019, vol. 95, no. 11, pp. 170-175. doi: https://doi.org/10.15199/48.2019.11.44.
23. Lai K., Lim S., Teh P., Yeap K. An Artificial Neural Network Approach to Predicting Electrostatic Separation Performance for Food Waste Recovery. *Polish Journal of Environmental Studies*, 2017, vol. 26, no. 4, pp. 1921-1926. doi: https://doi.org/10.15244/pjoes/68963.
24. Achouri I.E., Zeghloul T., Medles K., Richard G., Nouri H., Dascalescu L. Tribo-aero-electrostatic separation of micronized waste plastics. *ESA '17 - Annual Meeting of the Electrostatics Society of America*, 2017, pp. 1-8. Available at: https://hal.science/hal-04427166 (Accessed 02 May 2025).
25. Ardakani A.H., Abdollahian S.A., Abdollahi F. NARX Transformer: A Dynamic Model for Leveraging Multicycle Data in Long-Term Battery State of Health Estimation. *IEEE Transactions on Instrumentation and Measurement*, 2024, vol. 73, pp. 1-8. doi: https://doi.org/10.1109/TIM.2024.3460947.
26. Ezzeldin R., Hatata A. Application of NARX neural network model for discharge prediction through lateral orifices. *Alexandria Engineering Journal*, 2018, vol. 57, no. 4, pp. 2991-2998. doi: https://doi.org/10.1016/j.aej.2018.04.001.
27. Chen C., Chen H., Shi J., Yue D., Shi G., Lyu D. Estimating Lithium-Ion Battery Health Status: A Temporal Deep Learning Approach With Uncertainty Representation. *IEEE Sensors Journal*, 2025, vol. 25, no. 14, pp. 26931-26943. doi: https://doi.org/10.1109/JSEN.2025.3572291.
28. Kalaycioglu S., de Ruiter A. Vibration Control of Satellite Antennas via NMPC and NARX Neural Networks. *IEEE Transactions on Aerospace and Electronic Systems*, 2025, vol. 61, no. 4, pp. 9406-9433. doi: https://doi.org/10.1109/TAES.2025.3551276.
29. Bouhamri N., Zelmat M.E., Tilmatine A. Micronized plastic waste recycling using two-disc tribo-electrostatic separation process. *Advanced Powder Technology*, 2019, vol. 30, no. 3, pp. 625-631. doi: https://doi.org/10.1016/j.apt.2018.12.012.
30. Messal S., Zeghloul T., Mekhalef-Benhafssa A., Medles K., Dascalescu L. Experimental study of a tribo-aero-electrostatic separator for finely-grinded matter. *Journal of Electrostatics*, 2017, vol. 89, pp. 59-68. doi: https://doi.org/10.1016/j.elstat.2017.08.004.
31. Zeghloul T., Mekhalef Benhafssa A., Richard G., Medles K., Dascalescu L. Effect of particle size on the tribo-aero-electrostatic separation of plastics. *Journal of Electrostatics*, 2017, vol. 88, pp. 24-28. doi: https://doi.org/10.1016/j.elstat.2016.12.003.
32. Achouri I.E., Zeghloul T., Richard G., Medles K., Nouri H., Dascalescu L. Factors that Influence the Performance of a Two-Rotating Disks-Type Tribo-Aero-Electrostatic Separator for Micronized WEEE. *IEEE Transactions on Industry Applications*, 2019, vol. 55, no. 1, pp. 802-811. doi: https://doi.org/10.1109/TIA.2018.2866546.
33. Mekhalef Benhafssa A., Zeghloul T., Aksa W., Medles K., Dascalescu L. Continuous operation of a fluidized-bed disk-type electrostatic separator for micronized plastic waste. *Waste Management*, 2018, vol. 79, pp. 763-769. doi: https://doi.org/10.1016/j.wasman.2018.08.044.
34. Sjoberg J. Neural networks for modelling and control of dynamic systems, M. Nørgaard, O. Ravn, N. K. Poulsen and L. K. Hansen, Springer, London, 2000, xiv+246pp. *International Journal of Robust and Nonlinear Control*, 2001, vol. 11, no. 9, pp. 881-882. doi: https://doi.org/10.1002/rnc.585.
35. Tsungnan Lin, Horne B.G., Tino P., Giles C.L. Learning long-term dependencies in NARX recurrent neural networks. *IEEE Transactions on Neural Networks*, 1996, vol. 7, no. 6, pp. 1329-1338. doi: https://doi.org/10.1109/72.548162.
36. Sola J., Sevilla J. Importance of input data normalization for the application of neural networks to complex industrial problems. *IEEE Transactions on Nuclear Science*, 1997, vol. 44, no. 3, pp. 1464-1468. doi: https://doi.org/10.1109/23.589532.
37. Salinas D., Flunkert V., Gasthaus J., Januschowski T. DeepAR: Probabilistic forecasting with autoregressive recurrent networks. *International Journal of Forecasting*, 2020, vol. 36, no. 3, pp. 1181-1191. doi: https://doi.org/10.1016/j.ijforecast.2019.07.001.
38. Qi M., Zhang G.P. An investigation of model selection criteria for neural network time series forecasting. *European Journal of Operational Research*, 2001, vol. 132, no. 3, pp. 666-680. doi: https://doi.org/10.1016/S0377-2217(00)00171-5.
39. Shrestha A., Mahmood A. Review of Deep Learning Algorithms and Architectures. *IEEE Access*, 2019, vol. 7, pp. 53040-53065. doi: https://doi.org/10.1109/ACCESS.2019.2912200.

Received 18.08.2025
Accepted 20.10.2025
Published 02.01.2026

Z. Ayache[1], *Assistant Lecturer,*
O. Dahou[2], *PhD, Associate Professor,*
[1] IRECOM Laboratory,
Djillali Liabes University of Sidi Bel-Abbes, Algeria,
e-mail: zouaoui.ayache@univ-sba.dz
[2] Electrical Engineering Department,
Mustapha Stambouli University of Mascara, Algeria,
e-mail: o.dahou@univ-mascara.dz (Corresponding Author)

How to cite this article:
Ayache Z., Dahou O. Development of a NARX neural network for a tribo-aero-electrostatic separator with rotating disk electrodes. *Electrical Engineering & Electromechanics*, 2026, no. 1, pp. 20-27. doi: https://doi.org/10.20998/2074-272X.2026.1.03